Osteoarthritis and Cartilage (2009) **17,** 1461–1468
© 2009 Osteoarthritis Research Society International. Published by Elsevier Ltd. All rights reserved.
doi:10.1016/j.joca.2009.04.021

Osteoarthritis and Cartilage

International Cartilage Repair Society

OARSI OSTEOARTHRITIS RESEARCH SOCIETY INTERNATIONAL

In situ deformation of cartilage in cyclically loaded tibiofemoral joints by displacement-encoded MRI

D. D. Chan†, C. P. Neu†* and M. L. Hull‡§

† *Weldon School of Biomedical Engineering, Purdue University, West Lafayette, IN 47907, United States*

‡ *Biomedical Engineering Graduate Group, University of California at Davis, Davis, CA 95616, United States*

§ *Department of Mechanical and Aeronautical Engineering, University of California at Davis, Davis, CA 95616, United States*

Summary

Objectives: Cartilage displacement and strain patterns were documented noninvasively in intact tibiofemoral joints *in situ* by magnetic resonance imaging (MRI). This study determined the number of compressive loading cycles required to precondition intact joints prior to imaging, the spatial distribution of displacements and strains in cartilage using displacement-encoded MRI, and the depth-dependency of these measures across specimens.

Design: Juvenile porcine tibiofemoral joints were cyclically compressed at one and two times body weight at 0.1 Hz to achieve a quasi-steady state load–displacement response. A 7.0 T MRI scanner was used for displacement-encoded imaging with stimulated echoes and a fast spin echo acquisition (DENSE-FSE) in eight intact joints. Two-dimensional displacements and strains were determined throughout the thickness of the tibial and femoral cartilage and then normalized over the tissue thickness.

Results: Two-dimensional displacements and strains were heterogeneous through the depth of femoral and tibial cartilage under cyclic compression. Strains in the loading direction were compressive and were maximal in the middle zone of femoral and tibial cartilage, and tensile strains were observed in the direction transverse to loading.

Conclusions: This study determined the depth-dependent displacements and strains in intact juvenile porcine tibiofemoral joints using displacement-encoded imaging. Displacement and strain distributions reflect the heterogeneous biochemistry of cartilage and the biomechanical response of the tissue to compression in the loading environment of an intact joint. This unique information about the biomechanics of cartilage has potential for comparisons of healthy and degenerated tissue and in the design of engineered replacement tissues.
© 2009 Osteoarthritis Research Society International. Published by Elsevier Ltd. All rights reserved.

Key words: Tibiofemoral cartilage, Deformation, Strain pattern, Magnetic resonance imaging, Noninvasive.

Introduction

Knowledge of deformations within the cartilage of intact joints is useful in the study of healthy and degenerated articular cartilage. Mechanical signals regulate gene expression and protein synthesis[1] and modulate the biosynthesis and degradation of various cartilage constitutive macromolecules[2]. Disruption of the structure and function of cartilage is characteristic of degenerative joint diseases like osteoarthritis, and chondrocyte metabolism correlates with cartilage degeneration[3]. In addition, restoration of physiologic strains in regenerated cartilage can be used as a design endpoint in the functional restoration by the engineered construct[4,5]. Although important information about the deformation of cartilage can be determined experimentally in explanted tissue, the intact joint environment is of utmost importance to the biological and mechanical behavior of articular cartilage. Considering the prevalence of osteoarthritis and the need to understand and replicate the unique properties of cartilage, the distribution of deformations and strains within the cartilage of an intact joint is of paramount importance to determine.

Various techniques can characterize deformation within tissue, but few are well-suited for determining deformations in an intact joint. Biomechanics methods, such as indentation[6–8] and video microscopy[9,10], provide important information about cartilage but typically assess cartilage only after removal from the joint. Various imaging techniques, on the other hand, can evaluate tissue less invasively. Ultrasound has been used to evaluate mechanical properties during osmotic swelling[11], with indentation[7], and under compression[12]. These techniques, however, still require proximity of the probe to the tissue of interest, requiring arthroscopy when used for intact joints. Although micro-computed tomography is capable of measuring the thickness and biochemical degeneration of cartilage[13], the authors are not aware of any applications of this technique to visualize depth-dependent deformation. Therefore, a truly noninvasive technique remains preferable for the examination of deformations within an intact joint.

Magnetic resonance imaging (MRI) is a noninvasive technique used previously to investigate the deformation of the articular surface[14,15] and cartilage volume changes[16]. However, these techniques do not capture deformation

*Address correspondence and reprint requests to: Corey P. Neu, Weldon School of Biomedical Engineering, Purdue University, 206 South Martin Jischke Drive, West Lafayette, IN 47907-2032, United States. Tel: 1-765-496-1426; Fax: 1-765-494-0902; E-mail: cpneu@purdue.edu

Received 2 December 2008; revision accepted 26 April 2009.

patterns within the tissue and provide only nominal strain information. Two other MRI techniques, cartilage deformation by tag registration[17] and phase-contrast MRI[18] have been used to evaluate the heterogeneous deformation patterns within full-thickness articular cartilage explants. The phase-contrast MRI method combines displacement-encoded imaging with stimulated echoes (DENSE) and a fast spin echo (FSE) acquisition to provide displacements at sub-pixel precision[18] and has been demonstrated in a single intact joint[19]. Because most MRI techniques require multiple excitations to acquire data for a complete image, tissue must either be statically loaded to equilibrium or cyclically loaded to achieve a quasi-steady state load–deformation response[20].

The purpose of this study was to document depth-dependent displacement and strains in the cartilage of intact tibiofemoral joints *in situ*. To this end, the specific objectives were threefold. The first was to determine the number of loading cycles required to achieve quasi-steady state load–deformation behavior in intact porcine tibiofemoral joints for different load levels. The second objective was to use DENSE-FSE to determine two-dimensional deformations and strains through the thickness of the tibial and femoral cartilage in multiple joints. A final objective was to compare deformations and strains across specimens to identify depth-dependent mechanical behavior in response to cyclic compression.

Methods

SPECIMEN PREPARATION

Fresh-frozen young porcine legs (approximately 4 weeks old) were obtained from a local abattoir and remained frozen until use. Subcutaneous soft tissue further than 3 cm from the joint line was removed, leaving the diaphyses clear of tissue for potting with polymethylmethacrylate into custom-machined end caps, which were positioned with the tibial end cap concentric to the tibial intermedullary canal. Each specimen was secured within the apparatus so that movement in all degrees of freedom, except compression–distraction, was restricted.

DESIGN DESCRIPTION

A loading apparatus was designed to cyclically compress an intact stifle within a 7.0 T MRI scanner (Bruker Medical GmbH, Ettlingen, Germany). The components of the apparatus were restricted to plastics and other non-ferromagnetic materials, with no metal located within the radiofrequency (RF) coil to minimize artifacts generated by local magnetic fields (Fig. 1). The loading apparatus was computer-controlled by an electro-pneumatics system[17] and cyclic compressive loads were applied with a custom-modified, double-acting pneumatic cylinder (Bimba Manufacturing Co, Monee, IL).

DETERMINATION OF CYCLES TO STEADY STATE

Eight joints were cyclically loaded with the custom apparatus for 1000 cycles at two times body weight and 0.1 Hz to determine the number of cycles required for quasi-steady state load–deformation behavior. The specimens were attached so that the tibia was fixed to the actuating piston rod, with the femur fixed to the apparatus (Fig. 1). Loads of 156 N were applied to replicate twice the body weight of a 4-week-old porcine (8 kg[21]) for 1.5 s each loading cycle[19,22]. Displacements of the tibia relative to the femur were measured using a laser displacement sensor (LB-081/1101(W), Keyence Corporation, Woodcliff Lake, NJ) during the loaded portion of every third loading cycle. These results were then compared to those of a previous study of joints loaded at one times body weight over 800 cycles[19]. Additional cycles were used for two times body weight because specimens subjected to higher load levels were expected to require additional cycles to reach quasi-steady state[20]. The specimens were considered to have reached a quasi-steady state load–deformation behavior when the linearly regressed slope of displacement with respect to time fell below a predetermined slope criterion[17]. In addition, a creep criterion required that, after quasi-steady state behavior is achieved, the standard deviation (SD) of displacements could not exceed half the spatial resolution[17].

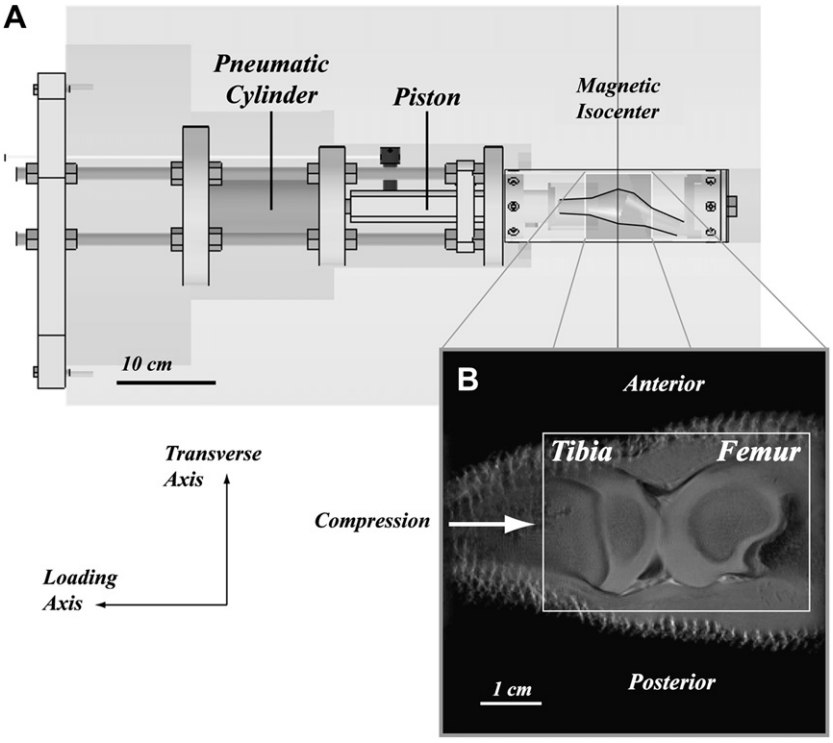

Fig. 1. Diagram of loading apparatus (A) and MR image of an intact porcine tibiofemoral joint (B). The loading apparatus (A) allowed for cyclic compression of an intact tibiofemoral joint in an MR scanner. The positioning of an intact joint through the magnetic isocenter of the MR scanner and an imaged slice taken through the joint are shown. Loading was applied to the tibia, which was held fixed to the actuating piston of the pneumatic cylinder. The inset box defines the cropped field of view shown in subsequent images.

DISPLACEMENT-ENCODED IMAGING

Eight additional intact tibiofemoral joints were used for displacement-encoded imaging with DENSE-FSE. Imaging was performed on a 7.0 T MR scanner with displacement-encoded imaging with stimulated echoes (DENSE[23]) and an FSE acquisition[18]. After selecting a sagittal slice through the widest part of the contact area in the medial condyle, cyclic compression was initiated. Displacement-encoded imaging did not commence until specimens were cyclically loaded for a number of cycles equal to the mean number of cycles required for quasi-steady state plus two SDs, as found above. Standard FSE sequences (3000 ms repetition time, 21.6 ms echo time, 256×256 pixel matrix size, 64×64-mm^2 field of view, 1.5 mm slice thickness) allowed for an estimation of the cartilage-on-cartilage contact area in both condyles.

The DENSE-FSE MRI sequence, employing image parameters as previously reported[19], was synchronized with the loading cycles using an electropneumatics control system (Fig. 2). During each 10-s cycle, a 90° RF pulse was followed by a phase-modulated 90° RF pulse, with the phase of the second RF pulse modulated to eliminate acquisition artifacts[24]. A displacement-encoding gradient was then applied between the first two RF pulses. The specimen was then loaded, and an equal displacement-encoded gradient was applied during the loading plateau, following a third 90° RF pulse. Displacement-encoded gradients were applied in frequency- and phase-encode directions, which correspond to loading and transverse directions. Imaging data were then acquired using FSE before the end of the loading plateau.

TWO-DIMENSIONAL DISPLACEMENTS AND STRAINS

Displacement and strain fields were determined in each of the eight juvenile porcine tibiofemoral joints using DENSE-FSE at one times body weight (78 N), because not all specimens loaded at two times body weight met the creep criterion (see Results). After image acquisition, software (Paravision, Bruker Medical GMBH, Ettlingen, Germany) was used to select spline-fit regions of interest that encompass the femoral and tibial cartilage in the loaded joint to create image masks for data analysis. For each scan set, RF-phase-modulated DENSE-FSE data were combined using the CANSEL method[24] prior to Fourier transformation. Phase was unwrapped using a region-growing algorithm, and the phase common to both reference and displacement-encoded images was eliminated by subtraction to determine displacement-encoded phase. Displacements for each pixel within the region of interest (Δx) were then directly calculated[18]. Strains were then computed from smoothed discrete displacement fields using a maximum likelihood estimation[25] for the Green–Lagrange strain tensor as previously reported[19].

To compare displacements and strains between specimens, the midpoint between the most anterior and posterior points of tibiofemoral contact was first identified. A line in the direction of loading and passing through the selected midpoint was then selected within the tibial and femoral cartilage [Fig. 3(B)]. Data along this line of interest were then interpolated using a spline fit to determine the displacements and strain for every 10% of the thickness through the cartilage. This allowed for displacements and strains along this line of interest to be compared between specimens. The thicknesses of the femoral and tibial cartilage were also measured along this line of interest. Both the sample mean and standard error were computed for the contact area on both medial and lateral contact surfaces, the depth of the cartilage along the lines of interest, and the displacements and strains also along the lines of interest.

STATISTICS

An unpaired two-sample Student's t test, assuming different variances, was used to determine whether the number of cycles to steady state between one and two times body weight was significantly different. All data are presented as a mean $\pm$ standard error, unless indicated as SD.

Results

DETERMINATION OF CYCLES TO STEADY STATE

Loading at two times body weight resulted in a significant increase in number of cycles to steady state ($P < 0.01$) compared to loading at one times body weight, which had required 224 ± 161 (SD) loading cycles to reach quasi-steady state[19]. Joints loaded to two times body weight met the predetermined slope criterion for quasi-steady state at 434 ± 142 (SD) loading cycles. However, four specimens loaded at this level did not meet the creep criterion, with a SD of displacements greater than half the spatial resolution (125 μm) after the quasi-steady state criterion was met. Therefore, joints in this study were cyclically loaded at one times body weight for 546 ($=224 + 2 \times 161$) cycles prior to any imaging, and results from specimens imaged with two times body weight cyclic compression were not reported.

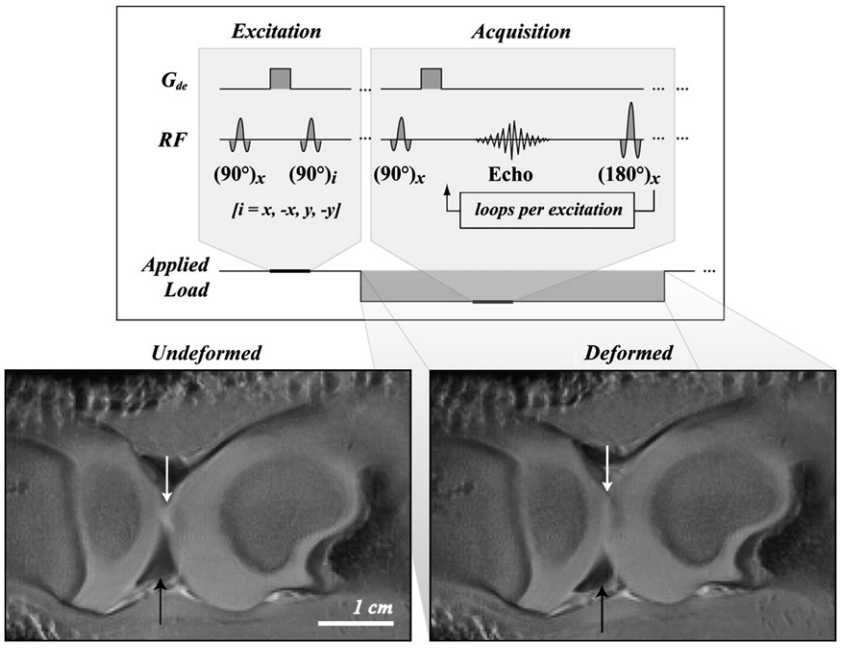

Fig. 2. DENSE-FSE imaging synchronized loading cycles and MR image actions. Displacement-encoded gradients were applied during excitation of the tissue and acquisition of image data, which occur before and during loading, respectively. The deformed specimen shows a widened area of contact (white arrows) and also motion of surrounding soft tissue, especially the meniscus (black arrows).

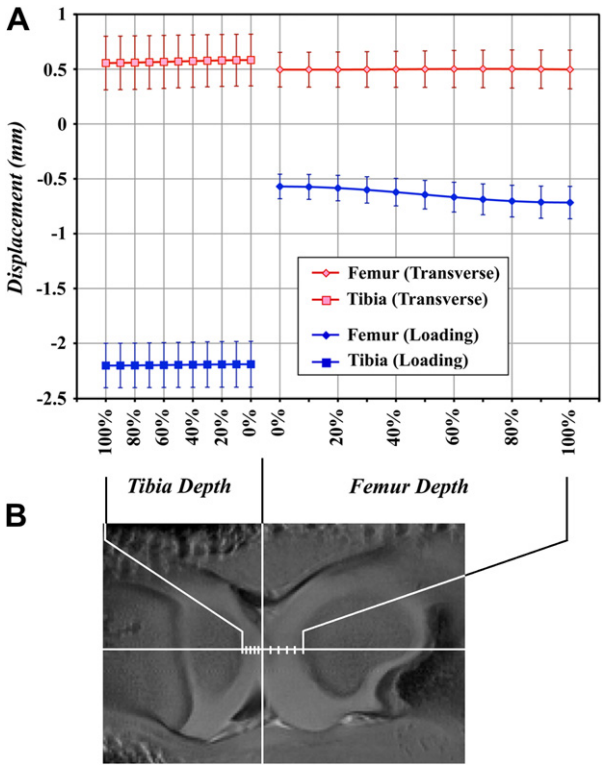

Fig. 3. Displacements in the loading and transverse directions for both the tibial and femoral cartilage included rigid body and internal motion. Tissue displacements as determined along a line of interest are shown with respect to the depth from the articulating surface (A). The line of interest was located parallel to the direction of loading and passed through the midpoint of the contact between the femoral and tibial cartilage. Displacements in the transverse and loading directions varied through the thickness. An MR image of a representative specimen (B) indicates the position of the line of interest as well as the locations of every 20% of the thickness of the tibial and femoral cartilage.

TWO-DIMENSIONAL DISPLACEMENTS AND STRAINS

Cartilage–cartilage contact area through the medial and lateral condyles as estimated to be 19.6 ± 2.2 mm^2 and 23.6 ± 1.5 mm^2, respectively, with an average combined area of 43.1 ± 3.3 mm^2. Tibial and femoral cartilage depth through the selected lines of interest averaged 2.9 ± 0.4 mm and 5.9 ± 0.3 mm, respectively, resulting in an average 0.5 ± 0.1 ratio of tibial to femoral cartilage thickness.

Heterogeneous displacement fields were observed in both the loading and transverse directions in femoral and tibial cartilage for all specimens (Fig. 3). Displacements in the loading direction in the tibial cartilage averaged -2.2 ± 0.2 mm along the line of interest through the entire depth of the tissue, although variations were seen in individual specimens. Femoral displacements in the loading direction increased in an absolute sense from -0.6 ± 0.1 mm at the surface (0% depth) to -0.7 ± 0.1 mm at the subchondral bone interface (100% depth). Femoral and tibial cartilage displacements in the transverse direction along the entire line of interest were 0.5 ± 0.2 mm and 0.6 ± 0.2 mm, respectively.

In one representative specimen (Fig. 4), strains were heterogeneous throughout the tibial and femoral cartilage. Maximal transverse strains were along the line of interest in the femoral cartilage but posterior to that line in the tibial cartilage. Maximal strains in the loading direction and in shear were found near the middle of the cartilage, also slightly posterior to the line of interest.

For the sample of eight specimens, strains in the loading direction were greatest at 50% of the thickness of the femoral cartilage, at a value of $-3.6\% \pm 1.0\%$, and at 50% of the total tibial thickness, with a value of $-0.4\% \pm 0.2\%$ (Fig. 5). Tensile strains in the transverse direction in the femur had a maximum of $3.0 \pm 0.4\%$ at 70% of the thickness of the cartilage from the surface. The maximum transverse strain in the tibial cartilage, at the subchondral bone interface, was $2.6 \pm 0.5\%$. Shear strains in the femoral cartilage were also maximal at the subchondral bone surface with values of $-1.0 \pm 0.3\%$. Shear in the tibial cartilage had a maximum of $-0.2 \pm 0.2\%$ at 50% of the depth.

Discussion

In this study, the heterogeneous two-dimensional deformations and strains of intact juvenile porcine tibiofemoral joints were determined using displacement-encoded MRI. Synchronized imaging and cyclic compression allowed for consistent image acquisition over multiple excitations after specimens were brought to a quasi-steady state load–deformation response. Displacement-encoded phase data of DENSE-FSE images were then used to determine deformation fields and compute strains. Displacement and strain values along a line through the contact area were normalized to the thickness of the cartilage for comparison.

Specimens were defined as having reached a quasi-steady state load–deformation response when their change in displacement over the total imaging time did not exceed half the imaging resolution[20]. True steady state load–deformation response can be achieved with cyclically loaded cartilage explants[17], but was not seen in intact joints used in this study, where there is a greater quantity and variety of viscoelastic tissues under load[20]. Nevertheless, because the joint achieves a quasi-steady state load–deformation response, it is reasonable to assume that all constituent tissues of the joint have also reached this criterion. Because the same quasi-steady state criterion was applied to sets of specimens loaded at one and two times body weight at the same loading frequency, the difference ($P < 0.01$) in the number of compressive load cycles to achieve the defined quasi-steady state lies in the differences between loading conditions. However, imaging at loads of two times body weight was excluded from this study because the entire joint failed to meet the creep criterion after a quasi-steady state response was achieved.

Reliability of DENSE-FSE can be expressed as the absolute precision and bias of this technique in measuring displacement and strain. The precision of DENSE-FSE is 65 μm in displacement and 0.2% strain[19], with no significant strain bias[18]. Because fluid motion could influence the measurement of displacements, the rate of fluid displacement[18] was estimated to be 0.53 μm/s, given an applied pressure of 1.9 MPa (a conservative estimate using the cartilage–cartilage contact area) and average thickness of tibial cartilage (2.9 mm). Because all imaging occurred within 1.5 s, fluid motion was negligible compared to the image spatial resolution and did not bias measured displacements.

The heterogeneous strain patterns determined in this study highlight the importance of the loading environment of an intact joint to the strain distribution. In newborn bovine

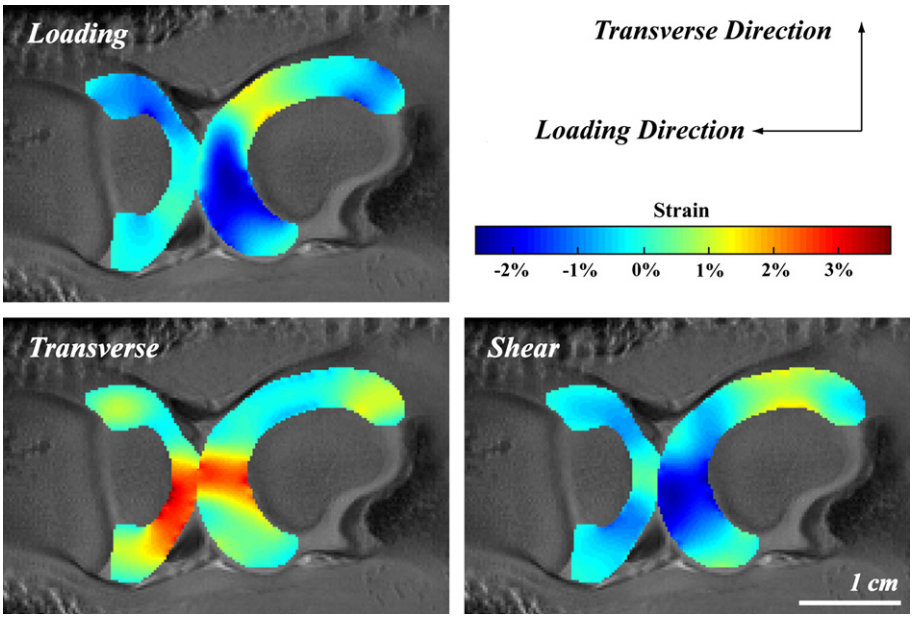

Fig. 4. Normal strains in the loading and transverse directions and shear strains for a representative specimen under cyclic compression at one times body weight. Displacements were noninvasively determined using DENSE-FSE, and then smoothed displacement fields were used to compute components of the Green–Lagrange strain tensor at each pixel location. Strains in the loading direction indicate compression near the tibiofemoral contact area, and tensile strains were observed in the direction transverse to the loading axis.

cartilage explants compressed between porous platens, axial strains were highest at the superficial zone and decreased nonlinearly through a 1-mm layer of cartilage[9], although the full cartilage depth was not investigated. Other studies have demonstrated maximal strains in the loading direction at the articular surface of juvenile[26,27] and adult bovine articular cartilage[26]. Another study showed axial compressive strains to be maximal in the middle of the full-thickness young bovine cartilage[18]. The current study also found compressive strains highest in the middle of the cartilage and lower at both the subchondral and articular surfaces. As discussed below, factors including unique joint geometry, heterogeneous material properties, and the role of other soft tissues in the joint (i.e., menisci, ligaments) in supporting and redistributing the load could affect the distribution of strains in the loading direction.

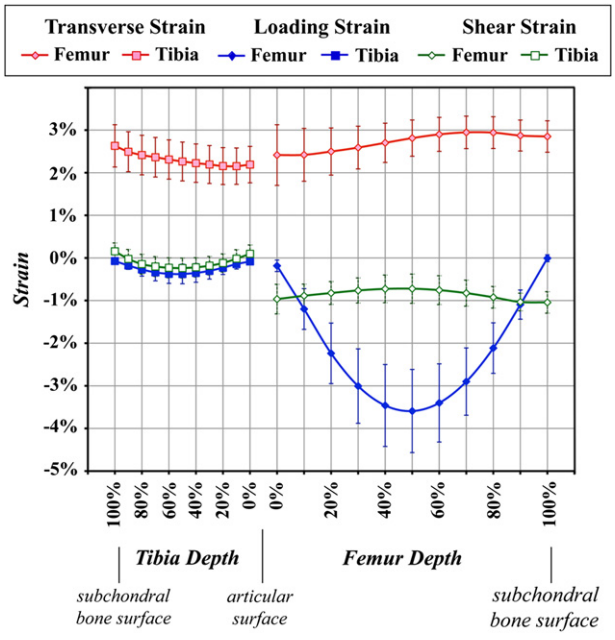

Fig. 5. Normal strains (in the transverse and loading directions) and shear strains varied with depth through the thickness of the cartilage. Strains were normalized to the thickness of the femoral and tibial cartilage from the articulating surface. Interpolated data are shown for every 10% of the thickness of the cartilage, with 100% at the subchondral surface of the region of interest.

Differences in peak strains and strain distributions in the transverse direction are also observed. Explant studies have shown that transverse strains are tensile and maximal at the articular surface[18,26,27]. In contrast, the transverse strains in this study, which were normalized to the depth of the cartilage, showed maxima at the tibial subchondral interface (Fig. 5) and within the thickness of the femoral cartilage, although transverse strains at all levels of depth were similar. Averaging over all specimens likely minimized detailed and individual strain features, perhaps also explaining the small difference between depths in the averages of transverse-direction strains.

Previous studies have also differed in their findings of the shear strain distributions in cartilage. One study found that shear was maximal at the subchondral interface of young bovine cartilage[27], while another found that the maximum shear occurred at the articular surface of immature cartilage[26]. Yet another study showed that shear strains were minimal through the thickness of the cartilage when compared to the magnitude of strains in the loading and transverse directions[18]. In our study, shear strains along the line of interest were close to zero in the tibial cartilage and were minimal in the femoral cartilage. Because shear strain distributions indicate the degree of matrix distortion during loading, smaller shear strains would be expected

where cartilage is distorted less. Differences in shear strain between depths were also small, similar to transverse-direction strains.

Strain patterns were attributed in part to the loading environment, as influenced by the geometry and mechanical properties of the surfaces in contact. Previous experimental studies were performed with explants in contact with flat and nonporous[18,26,27] or porous[9] surfaces, which are significantly stiffer than tissue within the joint. In our study, all structures within the joint were intact, preserving joint geometry and cartilage contact with other tissues of the joint. Therefore, contact with surrounding tissues, especially the opposing cartilage and menisci, should be considered in the comparison of strains in an intact joint vs an isolated explant.

Another contributing factor to strain patterns could be the age of the animals used in this study. The solid matrix becomes denser, tissue thickness decreases, and zonal variations become more apparent at approximately 1–3 months in porcine[28]. Because the specimens in this study lie in this age range, it is reasonable that zonal variations in mechanical properties are not as well defined as those observed in adults. Also, because this age range marks a period of rapid changes in the joint, much of the variance in displacements and strains can be attributed to biological heterogeneity. Therefore, differences in contact geometry as well as age- and depth-dependent cartilage properties create a unique loading environment and could explain the variations in measured peak displacement and strains.

Compared to unconfined compression testing of a cartilage explant, the cyclic loading of intact tibiofemoral joints poses a new array of challenges. As discussed previously, the presence of other tissues in the joint affects the ability of the entire joint to reach a quasi-steady state load–deformation response[20]. As opposed to explant experiments, there are various contacting surfaces in the joint, including the cartilage–cartilage and the cartilage–meniscus interfaces, so load can be transmitted through soft tissues other than cartilage. Therefore, loads are distributed differently within an intact joint compared to unidirectional compression of cartilage explants. Even between similar specimens, strain patterns can differ due to biological heterogeneity, as discussed previously. Additionally, testing an intact tibiofemoral joint involves the application of load through the tibia, and rigid body motion must be considered in the interpretation of displacement results. This is especially important if there is minimal contact between tibia and femur during the unloaded portion of each loading cycle. The challenges in measuring the mechanical response of intact joints, however, are offset by the advantages gained from the nondestructive determination of depth-dependent displacements within an articulating joint.

Determination of the deformations and strains of articular cartilage in intact joints is useful in many respects. The magnitude and variations in normal deformations and strains of intact joints can be used as baselines in studies comparing degenerated or damaged tissue in animal models. In particular, evaluation of changes in intact joints, rather than those in cartilage explants or tissue cultures, can reveal changes unique to degeneration of the whole joint. Comparison of the mechanical environment and tissue remodeling could reveal mechanisms of interaction between physical signals and biochemical changes[29,30]. Detailed deformation fields are also useful for determining and reproducing the biomechanical stimuli that affect individual chondrocytes, information that is particularly advantageous in engineering tissues for articular cartilage repair[31].

MRI, and displacement-encoded imaging in particular, offers various advantages in computing displacement and strain distributions in cartilage. While optical imaging methods are able to characterize deformations and strains throughout the thickness of a tissue, these techniques require the isolation of tissue from its physiologic environment[10,26,32]. On the other hand, MRI is a noninvasive technique that can be used to visualize the deformation of tissue without disrupting its surroundings. Previous MRI studies include those that compare the thicknesses of unloaded and loaded cartilage[33,34], track the displacement of taglines within the volume of the tissue[27], and use texture correlation to estimate deformation fields[35]. The change in thickness or volume, however, does not fully characterize the mechanical changes that occur within the tissue. Tagline tracing and texture correlation allow for identification of depth-dependent characteristics, but interpolation remains necessary to determine the motion of the entire region of interest, limiting these techniques in their resolution. One of the chief advantages of DENSE-FSE is that it enables the measurement of displacement for individual pixels throughout the tissue[18].

Among a plethora of applications, determination of detailed displacement and strain distributions is important for the validation of mathematical models. Previous finite element contact models of biphasic cartilage layers[36–39] have provided insight into the modes of load support[37], the importance of anisotropic[36] and depth-dependent[38] material properties, and the role of cartilage surface geometry[39], despite simplifications of cartilage morphology and contact geometry. Whole joint models offer additional information about tissue contact within intact joints[40–42], although validation of the modeled mechanical response remains difficult and has been constrained to nominal thickness changes[40]. Heterogeneous tissue displacements and strain distributions measured noninvasively and within intact joints, such as those reported in this study, can thus be used to validate future cartilage contact models[26,42].

While DENSE-FSE has determined strains through the thickness of intact joints, there are limitations that must be considered as this technique is advanced. The joints used in this study are from a juvenile animal model because of the physical (small size) constraints of the MR system used for this study. Despite studies that show similarity in adult and juvenile strain patterns[26], there may still be limits to the applicability of the deformation and strain fields in juvenile joints in comparison with adult cartilage. To achieve the quasi-steady state load-displacement response required for our study, a cyclic loading and unloading frequency was used that was typically lower than that observed during walking. Thus the deformations observed herein may be different from those during walking. Additionally, because a quasi-steady state is used as the defining point for initiation of imaging, creep in the intact joint may still occur over longer lengths of time depending on the loading conditions. This was seen in joints cyclically loaded at two times body weight (imaging results not presented) when that group failed to meet the creep criterion. Another limitation is the time required for the specimens to reach a quasi-steady state response followed by imaging time for a single slice of interest at an adequate signal-to-noise ratio. More extensive comparisons of displacements and strains between different joints are also necessary to better distinguish variations in the cartilage loading environment and mechanical properties. Lastly, although DENSE-FSE

can be used to determine three-dimensional displacements and strains, this study was limited to two-dimensions because of imaging time constraints. Three-dimensional strain fields in the articular cartilage of an intact joint would be a next natural step with displacement-encoded imaging. Faster image acquisition is necessary to allow additional images to be acquired within reasonable times at the same signal-to-noise. A faster imaging method would also improve possibilities of translating this technique to *in vivo* for human clinical research.

In conclusion, this study has characterized the heterogeneous two-dimensional deformation and strains in the cartilage of intact juvenile porcine tibiofemoral joints. Heterogeneous strain distributions are attributed to depth-dependent properties of cartilage and the loading environment of an intact joint. Displacement-encoded imaging in intact joints offers an improvement over previous studies of cartilage explants and also provides more detailed deformation fields compared to MR techniques that examine only nominal changes. This method has potential for validation of mathematical models and studies of damaged and degenerated cartilage. Further development of displacement-encoded imaging shows potential for *in vivo* research because the noninvasive nature of MRI is well-suited for longitudinal studies.

Conflict of interest

The authors have no conflict of interest.

Acknowledgments

The authors gratefully acknowledge funding from the National Institutes of Health (NIBIB 1F32 EB003371-01A1) and the UC Davis Nuclear Magnetic Resonance Facility.

References

1. Smith RL, Rusk SF, Ellison BE, Wessells P, Tsuchiya K, Carter DR, *et al.* In vitro stimulation of articular chondrocyte mRNA and extracellular matrix synthesis by hydrostatic pressure. J Orthop Res 1996;14:53–60.
2. Ikenoue T, Trindade MC, Lee MS, Lin EY, Schurman DJ, Goodman SB, *et al.* Mechanoregulation of human articular chondrocyte aggrecan and type II collagen expression by intermittent hydrostatic pressure in vitro. J Orthop Res 2003;21:110–6.
3. Aigner T, Kurz B, Fukui N, Sandell L. Roles of chondrocytes in the pathogenesis of osteoarthritis. Curr Opin Rheumatol 2002;14:578–84.
4. Butler DL, Goldstein SA, Guilak F. Functional tissue engineering: the role of biomechanics. J Biomech Eng 2000;122:570–5.
5. Hung CT, Mauck RL, Wang CC, Lima EG, Ateshian GA. A paradigm for functional tissue engineering of articular cartilage via applied physiologic deformational loading. Ann Biomed Eng 2004;32:35–49.
6. Han SK, Federico S, Grillo A, Giaquinta G, Herzog W. The mechanical behaviour of chondrocytes predicted with a micro-structural model of articular cartilage. Biomech Model Mechanobiol 2007;6:139–50.
7. Kiviranta P, Lammentausta E, Toyras J, Kiviranta I, Jurvelin JS. Indentation diagnostics of cartilage degeneration. Osteoarthritis Cartilage 2008;16:796–804.
8. Lu XL, Sun DD, Guo XE, Chen FH, Lai WM, Mow VC. Indentation determined mechanoelectrochemical properties and fixed charge density of articular cartilage. Ann Biomed Eng 2004;32:370–9.
9. Klein TJ, Chaudhry M, Bae WC, Sah RL. Depth-dependent biomechanical and biochemical properties of fetal, newborn, and tissue-engineered articular cartilage. J Biomech 2007;40:182–90.
10. Schinagl RM, Gurskis D, Chen AC, Sah RL. Depth-dependent confined compression modulus of full-thickness bovine articular cartilage. J Orthop Res 1997;15:499–506.
11. Wang Q, Zheng YP, Niu HJ, Mak AF. Extraction of mechanical properties of articular cartilage from osmotic swelling behavior monitored using high frequency ultrasound. J Biomech Eng 2007;129:413–22.
12. Zheng YP, Niu HJ, Arthur Mak FT, Huang YP. Ultrasonic measurement of depth-dependent transient behaviors of articular cartilage under compression. J Biomech 2005;38:1830–7.
13. Piscaer TM, Waarsing JH, Kops N, Pavljasevic P, Verhaar JA, van Osch GJ, *et al.* In vivo imaging of cartilage degeneration using muCT-arthrography. Osteoarthritis Cartilage 2008;16:1011–7.
14. Herberhold C, Faber S, Stammberger T, Steinlechner M, Putz R, Englmeier KH, *et al.* In situ measurement of articular cartilage deformation in intact femoropatellar joints under static loading. J Biomech 1999;32:1287–95.
15. Herberhold C, Stammberger T, Faber S, Putz R, Englmeier KH, Reiser M, *et al.* An MR-based technique for quantifying the deformation of articular cartilage during mechanical loading in an intact cadaver joint. Magn Reson Med 1998;39:843–50.
16. Eckstein F, Lemberger B, Stammberger T, Englmeier KH, Reiser M. Patellar cartilage deformation in vivo after static versus dynamic loading. J Biomech 2000;33:819–25.
17. Neu CP, Hull ML. Toward an MRI-based method to measure non-uniform cartilage deformation: an MRI-cyclic loading apparatus system and steady-state cyclic displacement of articular cartilage under compressive loading. J Biomech Eng 2003;125:180–8.
18. Neu CP, Walton JH. Displacement encoding for the measurement of cartilage deformation. Magn Reson Med 2008;59:149–55.
19. Chan DD, Neu CP, Hull ML. Articular cartilage deformation determined in an intact tibiofemoral joint by displacement-encoded imaging. Magn Reson Med 2009;61:989–93.
20. Martin KJ, Neu CP, Hull ML. Steady state displacement response of whole human cadaveric knees in an MRI scanner. J Biomech Eng (In press).
21. Poore KR, Forhead AJ, Gardner DS, Giussani DA, Fowden AL. The effects of birth weight on basal cardiovascular function in pigs at 3 months of age. J Physiol 2002;539:969–78.
22. Martin KJ, Neu CP, Hull ML. An MRI-based method to align the compressive loading axis for human cadaveric knees. J Biomech Eng 2007;129:855–62.
23. Aletras AH, Ding S, Balaban RS, Wen H. DENSE: displacement encoding with stimulated echoes in cardiac functional MRI. J Magn Reson 1999;137:247–52.
24. Epstein FH, Gilson WD. Displacement-encoded cardiac MRI using cosine and sine modulation to eliminate (CANSEL) artifact-generating echoes. Magn Reson Med 2004;52:774–81.
25. Geers MGD, de Borst R, Brekelmans WAM. Computing strain fields from discrete displacement fields in 2D-solids. Int J Solids Struct 1996;33:4293–307.
26. Canal CE, Hung CT, Ateshian GA. Two-dimensional strain fields on the cross-section of the bovine humeral head under contact loading. J Biomech 2008;41:3145–51.
27. Neu CP, Hull ML, Walton JH. Heterogeneous three-dimensional strain fields during unconfined cyclic compression in bovine articular cartilage explants. J Orthop Res 2005;23:1390–8.
28. Keinan-Adamsky K, Shinar H, Navon G. Multinuclear NMR and MRI studies of the maturation of pig articular cartilage. Magn Reson Med 2006;55:532–40.
29. Grodzinsky AJ, Levenston ME, Jin M, Frank EH. Cartilage tissue remodeling in response to mechanical forces. Annu Rev Biomed Eng 2000;2:691–713.
30. Szafranski JD, Grodzinsky AJ, Burger E, Gaschen V, Hung HH, Hunziker EB. Chondrocyte mechanotransduction: effects of compression on deformation of intracellular organelles and relevance to cellular biosynthesis. Osteoarthritis Cartilage 2004;12:937–46.
31. Shieh AC, Athanasiou KA. Principles of cell mechanics for cartilage tissue engineering. Ann Biomed Eng 2003;31:1–11.
32. Wang CC, Deng JM, Ateshian GA, Hung CT. An automated approach for direct measurement of two-dimensional strain distributions within articular cartilage under unconfined compression. J Biomech Eng 2002;124:557–67.
33. Eckstein F, Lemberger B, Gratzke C, Hudelmaier M, Glaser C, Englmeier KH, *et al.* In vivo cartilage deformation after different types of activity and its dependence on physical training status. Ann Rheum Dis 2005;64:291–5.
34. Song Y, Greve JM, Carter DR, Koo S, Giori NJ. Articular cartilage MR imaging and thickness mapping of a loaded knee joint before and after meniscectomy. Osteoarthritis Cartilage 2006;14:728–37.
35. O'Connell GD, Johannessen W, Vresilovic EJ, Elliott DM. Human internal disc strains in axial compression measured noninvasively using magnetic resonance imaging. Spine 2007;32:2860–8.
36. Donzelli PS, Spilker RL, Ateshian GA, Mow VC. Contact analysis of biphasic transversely isotropic cartilage layers and correlations with tissue failure. J Biomech 1999;32:1037–47.
37. Ateshian GA, Lai WM, Zhu WB, Mow VC. An asymptotic solution for the contact of two biphasic cartilage layers. J Biomech 1994;27:1347–60.

38. Krishnan R, Park S, Eckstein F, Ateshian G. Inhomogeneous cartilage properties enhance superficial interstitial fluid support and frictional properties, but do not provide a homogeneous state of stress. J Biomech Eng 2003;125:569.
39. Han SK, Federico S, Epstein M, Herzog W. An articular cartilage contact model based on real surface geometry. J Biomech 2005;38:179–84.
40. Li G, DeFrate LE, Park SE, Gill TJ, Rubash HE. In vivo articular cartilage contact kinematics of the knee: an investigation using dual-orthogonal fluoroscopy and magnetic resonance image-based computer models. Am J Sports Med 2005;33:102–7.
41. Haut Donahue TL, Hull ML, Rashid MM, Jacobs CR. A finite element model of the human knee joint for the study of tibio-femoral contact. J Biomech Eng 2002;124:273–80.
42. Dunbar Jr WL, Un K, Donzelli PS, Spilker RL. An evaluation of three-dimensional diarthrodial joint contact using penetration data and the finite element method. J Biomech Eng 2001;123:333–40.